Article:
Nkiaka, E orcid.org/0000-0001-7362-9430 (2022) Water security assessment in ungauged regions using the water balance and water footprint concepts and satellite observations. Hydrology Research, 53 (2). pp. 336-352. ISSN 0029-1277

https://doi.org/10.2166/nh.2022.124

Hydrology Research

Hydrology Research Vol 53 No 2, 336 doi: 10.2166/nh.2022.124

Water security assessment in ungauged regions using the water balance and water footprint concepts and satellite observations

Elias Nkiaka

Department of Geography, University of Sheffield, Sheffield S10 2TN, UK
E-mail: e.nkiaka@sheffield.ac.uk

EN, 0000-0001-7362-9430

ABSTRACT

Water security assessments often rely on outputs from hydrological models that are applicable only in gauged regions where there are river discharge data to constrain the models. Therefore, there is an urgent need to explore new methods for assessing water security in ungauged regions. This study proposes the use of the water balance and water footprint concepts and satellite observations to assess water security in Anglophone Cameroon, which is an example of a typically ungauged region. Specifically, the study assesses demand-driven water scarcity in terms of blue and green water scarcities and population-driven water scarcity quantified using the Falkenmark index across all districts in Anglophone Cameroon. The study also performs a spatiotemporal trend analysis of precipitation and temperature in the study area using the Mann–Kendall test. Precipitation trend analysis returns varying strengths and magnitudes for different districts unlike temperature which demonstrates an upward trend in all districts. The water security assessment shows that blue water scarcity is substantially low across most districts, whereas population-driven water scarcity is observed in densely populated districts ($<$1,700 m^3/capita/year). The results from this study suggest that the proposed method may be used to assess water security in ungauged regions irrespective of climate or population size.

Key words: blue water scarcity, evapotranspiration, Falkenmark index, green water scarcity, soil moisture storage

HIGHLIGHTS

- A methodology to identify water scarcity hotpots in ungauged regions was proposed.
- The method was used to demonstrate that the population-driven blue water scarcity is high in urban areas.
- The methodology also revealed areas that may be suitable for agricultural expansion to enhance food security.

GRAPHICAL ABSTRACT

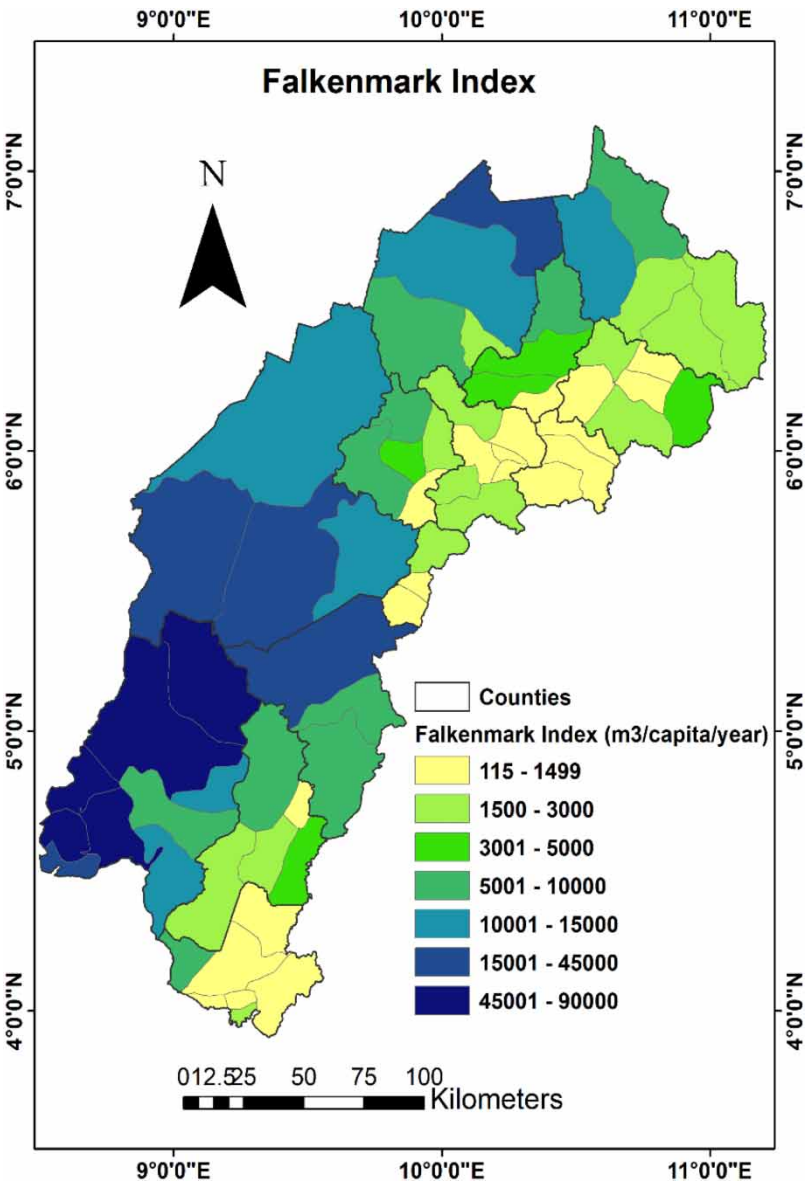

1. INTRODUCTION

The availability of water resources for human use, agriculture, and ecosystem sustainability is under severe threat from climate change and variability, rapid urbanisation, changing lifestyle, population, and economic growth, leading to competition among different water-use sectors (Flörke *et al.* 2018; Brown *et al.* 2019). Increasing surface temperatures caused by global warming are also expected to substantially increase evaporative demand and the demand for water in agriculture, industries, households, and power production, further exacerbating water scarcity (Gosling & Arnell 2016). Considering the multiple factors reinforcing global water scarcity, assessing water availability and the drivers of water scarcity have become critical for enhancing water security at different scales.

As an emerging concept, the framing of water security differs among different stakeholders, with scientists mostly focusing on water availability, scarcity, accessibility, quality, governance, and sustainability (Hailu *et al.* 2019). This study focuses on water availability, considering that it is critical for human and ecosystem functioning (Baggio *et al.* 2021). Different techniques exist for quantifying water availability, with the most common being the application of hydrological models.

While hydrological modelling remains the most widely used method for quantifying water resources, other approaches for assessing water availability have also been developed, such as the Falkenmark index (Falkenmark *et al.* 1989) and the water footprint concept (Hoekstra *et al.* 2011). Another method for assessing water availability is the life cycle assessment, which evaluates the impact of water consumption based on available water remaining per unit of surface in a given watershed relative to the world average using a consensus methodology that calculates the water scarcity footprint based on ISO14046 (ISO 2014; Boulay *et al.* 2018). This study adopts the Falkenmark index and the water footprint concept to assess water security. The Falkenmark index is defined as the total water resources that are available to the population of a given area (district, county, and country) at a given time. The Falkenmark index is useful for establishing the link between population growth and water scarcity. The water footprint is the total volume of freshwater that is used to produce the goods and services consumed by an individual or a community (Hoekstra 2017). The water footprint concept can be used to quantify water scarcity at different scales based on the volume of available water to the volume consumed and, as such, it can be used to identify water scarcity hotspots, prioritise management decisions, and assess sustainability (Mekonnen & Hoekstra 2016; Veettil & Mishra 2020).

Furthermore, the water footprint concept explicitly considers the different components of water availability, including green and blue water. Blue water (BW) is defined as water flowing through the surface and groundwater, which is stored in lakes, reservoirs, and aquifers and can be directly abstracted for human use; green water (GW) is the portion of precipitation that is stored in the soil and vegetation canopy and eventually returns to the atmosphere through evaporation from the surface or transpiration from vegetation (Rodrigues *et al.* 2014). Accordingly, the blue water footprint refers to human water consumption from blue sources and is quantified based on the volume of surface and groundwater consumed as a result of the production of goods and services such as domestic and industrial water consumption. The green water footprint refers to the consumption of GW resources, for example, through evapotranspiration from agriculture, grassland, and forest areas (Rodrigues *et al.* 2014; Veettil & Mishra 2020).

Different hydrological modelling studies have been used to assess blue and green water scarcities. For example, the soil and water assessment tool (SWAT) has been used to quantify blue and green water scarcities at the basin scale (Rodrigues *et al.* 2014; D'Ambrosio *et al.* 2020). Veettil & Mishra (2020) used outputs from the variable infiltration capacity (VIC) model to assess blue and green water scarcities across the contiguous USA. Mekonnen & Hoekstra (2016) estimated global blue water availability (BWA) using outputs from a global hydrological model. Several early studies relied on outputs from hydrological models to assess blue and green water scarcities. However, the application of hydrological models is limited to areas with observed river discharge data, which is crucial for constraining the models.

This implies that hydrological models may not be appropriate for assessing blue and green water scarcities in ungauged regions, whereas outputs from global hydrological models may be too coarse to be used at the local scale. Therefore, there is an urgent need to adopt new approaches for assessing blue and green water scarcities in ungauged regions. This study proposes the use of the water balance and water footprint concepts and satellite observations to assess blue and green water scarcities in ungauged regions. To achieve this, the study explores the numerous advantages of satellite observations, which include providing free, high spatial resolution and long-term homogeneous data for previously unmonitored areas at scales that are appropriate for water security assessments (Sheffield *et al.* 2018). The water balance concept has been widely used in several studies around the world to (1) validate global evapotranspiration estimates (Weerasinghe *et al.* 2020), (2) validate monthly terrestrial water storage (Xie *et al.* 2021), and (3) estimate water availability in ungauged basins (Simons *et al.* 2016; Rungee *et al.* 2021). Given that precipitation and temperature are important climatic variables underpinning water availability, this study also conducts a spatiotemporal trend analysis of precipitation and temperature over the study area, considering that there are no previous studies (to the best of my knowledge) covering all the districts in Anglophone Cameroon.

Therefore, the objectives of this study are to (1) conduct a spatiotemporal trend analysis of precipitation and temperature across all districts in Anglophone Cameroon; (2) combine the water balance and water footprint concepts and satellite observations to estimate water availability across all districts in Anglophone Cameroon; and (3) assess demand-driven water scarcity in terms of blue and green water scarcities and population-driven water scarcity quantified using the Falkenmark index. The objectives of this study are in line with recent calls to identify water scarcity hotspots at the local scale to support effective decision-making (Quinteiro *et al.* 2019; Nkiaka *et al.* 2021a).

The paper is structured as follows: section 2 provides a brief description of the study area and the research methodology. The results of geostatistical analyses are presented in section 3. A discussion on the results obtained and their implication on water security in the study area and finally the main conclusions from the study are presented in section 5.

2. MATERIALS AND METHODS

2.1. Study area

The study area is the English-speaking part of Cameroon, which is generally referred to as Anglophone Cameroon. It covers an area of about 43,000 km^2, is made up of the northwest and southwest regions, and consists of 13 counties and 65 administrative districts with an estimated population of 8 million (Figure 1). Agriculture is the main economic activity, with several large-scale agro-industrial complexes specialising in the production of rubber, oil palm, banana, tea, and rice. There are also several small-scale private plantations involved in the production of rubber, cocoa, coffee, rice, plantains, and palm oil. Anglophone Cameroon is the main breadbasket of Cameroon, supplying the country with food crops such as plantains, potatoes, bananas, cassava, rice, taro, beans, yams, maize, groundnuts, and a wide variety of fresh vegetables. Other economic activities include cattle rearing, artisanal fishing, and timber harvesting.

Although the area has a dense hydrographic network (Figure 1), to the best of my knowledge, there are no operational hydrometric stations, and access to rain gauge data has been hindered by an ongoing armed conflict. There are several volcanic lakes in the study area, with the most conspicuous being Lake Nyos, which exploded in August 1986 killing thousands of people and millions of cattle due to a limnic eruption (Halbwachs *et al.* 2020). Elevation ranges from 0 to 4,100 m.a.s.l. with several high peaks located along the Cameroon Volcanic Line. Some of the peaks include Fako Mountain (4,100 m), which is the highest peak in Central and West Africa, Mount Oku (3,011 m), and the Bamenda and Lebialem highlands. According to Köeppen–Geiger's climate classification for Africa, the southwest and a part of the northwest have a monsoon climate with the dense forest vegetation cover, whereas the rest of the northwest is dominated by tropical savannah climate and vegetation (Peel *et al.* 2007). Rainfall in the study area is strongly influenced by elevation variation (Vondou *et al.* 2018).

As the main breadbasket of Cameroon, there is a little understanding of hydroclimatic changes across Anglophone Cameroon, with often fragmented evidence on the impact of climate change and variability and population growth on water security. The analyses performed herein will be used as a foundation for future studies to simulate and predict the impact of climate change and variability, land-use change, and population growth on water and food security in the study area.

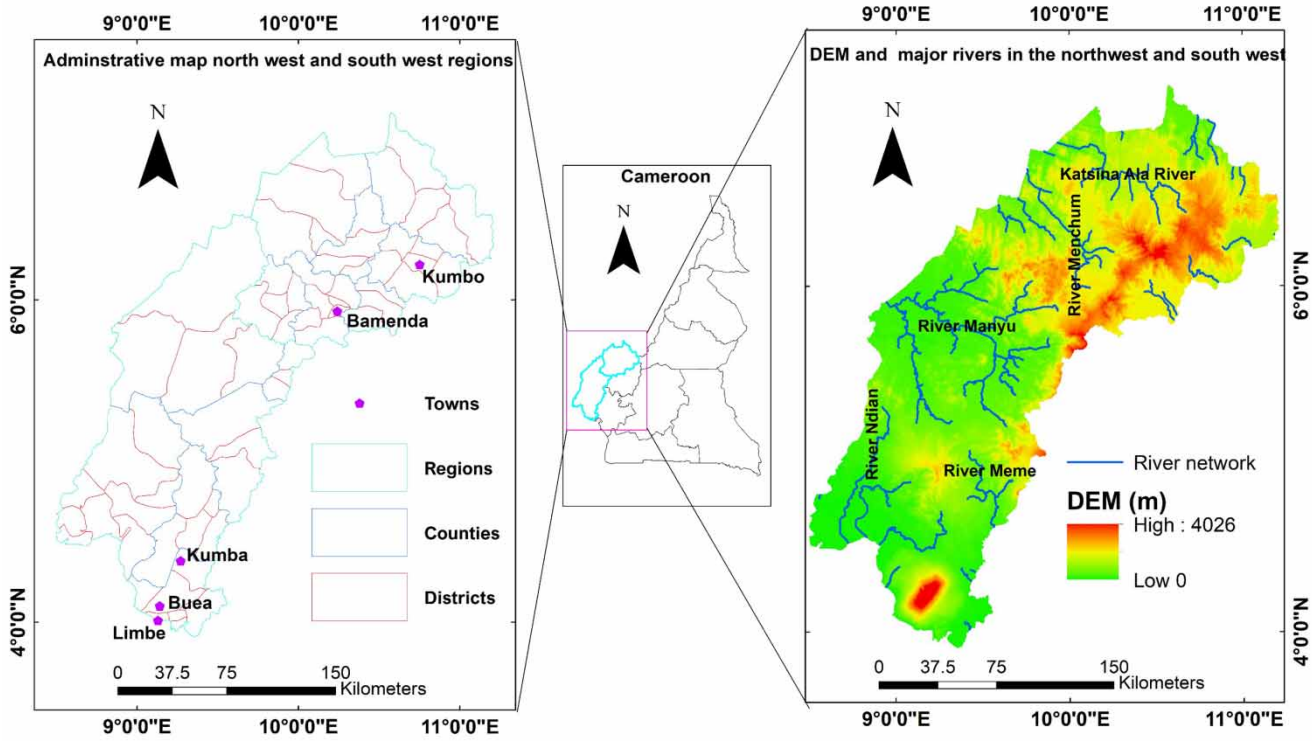

Figure 1 | Map of the study area showing the administrative setup and the DEM with the river network. DEM, digital elevation model. A full map of the study area with names of the districts and counties is available in Appendix A.

2.2. Datasets

This study makes use of satellite datasets derived from different sources. Precipitation estimates were obtained from the Climate Hazards Group InfraRed Precipitation with Station (CHIRPS). Temperature data were obtained from TerraClimate, a high-resolution global dataset of monthly climate and climatic water balance estimates. Evapotranspiration and soil moisture estimates were obtained from the Global Land Evaporation Amsterdam Model (GLEAM 3.5a).

2.2.1. CHIRPS precipitation

CHIRPS precipitation is produced by collaboration between Climate Hazards Group, the United States Geological Survey and Earth Resources Observation and Science Centre. It has a quasi-global coverage gridded at 0.05°×0.05°, spanning the period from 1981 to present at a daily timescale (Funk *et al.* 2015). CHIRPS precipitation is produced by using the Tropical Rainfall Measuring Mission Multi-Satellite Precipitation Analysis version 7 (TMPA-3B42-v7) to calibrate global Cold Cloud Duration (CCD) rainfall estimates. The dataset was explicitly designed taking into consideration the weaknesses of the existing products. As such, CHIRPS blends gauge and satellite precipitation covering most global land regions, and it has low latency, high resolution, low bias, and a long period of record (Funk *et al.* 2015). CHIRPS precipitation estimates have been validated across different regions in Africa (Dinku *et al.* 2018; Satgé *et al.* 2020). It has also been used in several studies in Africa, e.g., (1) to analyse long-term trends in precipitation (Muthoni *et al.* 2019; Alemu & Bawoke 2020), (2) for hydrological modelling (Dembélé *et al.* 2020; Larbi *et al.* 2020), (3) for flood studies (Elagib *et al.* 2021), and (4) to evaluate the drivers of flood events (Tramblay *et al.* 2021). CHIRPS data were downloaded free of charge from https://climateserv.servirglobal.net.

2.2.2. TerraClimate data

TerraClimate (TC) is a high-resolution climate dataset obtained by merging WorldClim version 2 (v2) global climate normals using the Japanese 55-year reanalysis (JRA-55) product and the Climate Research Unit time series data version 4 (Abatzoglou *et al.* 2018). The WorldClim v2 is a gridded dataset that uses Moderate Resolution Infrared Spectroradiometer (MODIS)-derived land surface temperature (max and min), cloud cover, and topographic features to develop monthly climate normal surfaces for global land surface at a high spatial resolution (1/24°). To produce TC time series, the high spatial resolution WorldClim v2 monthly climate normals are used to climatologically interpolate coarser resolution monthly climate anomalies from CRU4.0 and JRA-55. The final product is a monthly time series comprising different water balance components and climatic variables, including precipitation, maximum and minimum temperatures, vapour pressure, solar radiation, and wind speed. Only temperature data from TC were used in this study due to their extensive validation across the world (Abatzoglou *et al.* 2018). TC temperature data have also been validated and used in trend analysis in West Africa (Muthoni 2020) and in the Bahamas (Spellman *et al.* 2021). TC data were downloaded free of charge from www.climatologylab.org/terraclimate.html.

2.2.3. GLEAM evapotranspiration and soil moisture estimates

The GLEAM is a process-based semi-empirical model used for estimating surface soil moisture, root-zone soil moisture, and terrestrial evaporation using satellite forcing data (Martens *et al.* 2017). In the GLEAM, the different components of the terrestrial evaporation (transpiration, bare soil evaporation, open-water evaporation, interception loss, and sublimation) are derived separately. The model uses the Priestley and Taylor equation to calculate potential evapotranspiration for four different pixel land-cover fractions, namely open water, low vegetation, tall vegetation, and bare soil. Estimates of potential evapotranspiration are then converted to actual transpiration by incorporating an evaporative stress factor obtained from microwave observations of vegetation optical depth (as a proxy for vegetation water content) and root-zone soil moisture (simulations) on the land-cover type. Soil moisture is calculated for each of these fractions separately and then aggregated to the scale of the pixel based on the fractional cover of each land-cover type. Root-zone soil moisture is calculated by using a multilayered water balance equation that uses snowmelt and net precipitation as inputs and drainage and evaporation as outputs. The depth of the root zone is a function of the land-cover type and comprises three model layers for the fraction of tall vegetation (0–10, 10–100, and 100–250 cm), two for the fraction of low vegetation (0–10 and 10–100 cm), and one for the fraction of bare soil (0–10 cm) (Martens *et al.* 2017). Two datasets are available from GLEAM version 3, namely GLEAM v3.5a and GLEAM v3.5b. GLEAM v3.5a is produced using radiation and air temperature data from ERA5, the latest version of MSWEP precipitation (v2.8), ESA-CCI soil moisture (v5.3), and VODCA Vegetation optical depth (Martens *et al.* 2017).

GLEAM v3.5a was adopted in this study, because it covers the longest available time period (1980–2020) at both monthly and annual timescales with a spatial resolution of 0.25°. This increases the usability of this product at the local scale compared with other products with coarser spatial resolutions and shorter timescales. In addition, GLEAM soil moisture and actual evapotranspiration (AET) estimates have been extensively validated across Africa (Majozi *et al.* 2017; Khosa *et al.* 2020; Weerasinghe *et al.* 2020) and also used for constraining hydrological models (Odusanya *et al.* 2019; Dembélé *et al.* 2020). GLEAM estimates have also been used to analyse spatiotemporal changes in evapotranspiration over China (Yang *et al.* 2018). GLEAM v3.5a estimates were downloaded for free from www.gleam.eu.

2.3. Methods

To obtain data for each satellite product, the values of all grid cells located within each district were averaged over the timescale of our analysis (January 1982–December 2020), and the same procedure was repeated for all datasets and for all districts.

2.3.1. Trend analysis

Seasonal precipitation was obtained by aggregating monthly precipitation for June, July, August, and September (JJAS), which is the peak rainy season in the study area, and for March, April, and May (MAM), which is the main cultivation season. Trend analysis was carried out using the Mann–Kendall test to detect the presence of monotonic trends in annual and seasonal precipitation and annual temperature timeseries in the study area. The Mann–Kendall test has been extensively used to analyse trends in hydroclimatic variables (Nkiaka *et al.* 2017). Trend magnitude was estimated using the non-parametric Sen slope estimator that is also widely used in climatic data analysis (Nkiaka *et al.* 2017). Trends were analysed at the 5% significance level. The coefficient of variation was used to measure the variability in annual and seasonal precipitation.

2.3.2. Water security assessments

2.3.2.1. GW availability. In this study, GW availability or storage refers to soil water available in the top 1-m of the soil profile. This estimate was obtained by adding GLEAM estimates of surface soil moisture (0–10 cm) and root-zone soil moisture (10–100 cm) for each district. This estimate represents the amount of soil moisture storage that is available to sustain the growth of crops and other vegetation including trees. GW scarcity for a given district 'x' at period 't' was calculated as the ratio between the green water footprint and GW availability using the following equation:

$$GW_{scarcity} = \frac{Greenwater\ footprint_{(x,t)}}{Greenwater\ availability_{(x,t)}} \tag{1}$$

where $GW_{scarcity}$ is the green water scarcity, $Greenwater\ availability_{(x,t)}$ is the soil moisture storage for a given district 'x' at period 't', and $Greenwater\ footprint_{(x,t)}$ is the AET from a given district 'x' at period 't'. Data for GW availability or storage and green water footprint (AET) were obtained from GLEAM 3.5a.

2.3.2.2. Blue water availability. BWA is the amount of water that can be abstracted from surface and groundwater without affecting aquatic ecosystems. Considering that there are no hydrometric stations in our study area, we adopted the water balance concept to estimate BWA in each district using satellite estimates of precipitation and AET. For a given district, the water balance accounts for different water fluxes over the district as follows:

$$P - ET - R = \frac{\partial S}{\partial t} \tag{2}$$

where P is the precipitation, ET is the evapotranspiration, R is the runoff, and $\partial S/\partial t$ is the change in storage over time in a given area, which can be considered to be negligible over a long time period exceeding 10 years (Weerasinghe *et al.* 2020; Xie *et al.* 2021). To estimate BWA in each district, we first calculated the total available water (TWA) by taking the difference between precipitation and AET as follows:

$$TWA_{(x,\,t)} = P_{(x,t)} - AET_{(x,t)} \tag{3}$$

where $TWA_{(x,t)}$ is the total available water for a given district 'x' at period 't', $P_{(x,t)}$ is the total precipitation recorded in district 'x' at period 't', and $AET_{(x,t)}$ is the actual evapotranspiration from district 'x' at period 't'. This is based on basic hydrological principles and mass conservation that, over a number of hydrological years, precipitation surplus (P–AET) should equal the discharge at the outlet of the catchment (Simons *et al.* 2016). A similar approach has been used to estimate water availability in other studies (e.g., Simons *et al.* 2016; Rungee *et al.* 2021). Another reason for adopting AET to estimate water availability is that both local climatic factors and physical catchment attributes such as soil type, land cover, and topography that influence evapotranspiration at a local scale are also taken into consideration (Jaramillo *et al.* 2018).

Considering environmental flow requirements (EFRs), BWA for each district was calculated as follows:

$$BWA_{(x,\,t)} = TWA_{(x,t)} - EFR_{(x,t)} \tag{4}$$

where $BWA_{(x,t)}$ is the blue water availability for a given district 'x' at period 't', $TWA_{(x,t)}$ is the total available water for district 'x' at period 't', and $EFR_{(x,t)}$ represents the environmental flow requirements for a given district 'x' at period 't'. The standard method was used to quantify EFRs. As such, 25% of the TWA can be considered to be appropriate for withdrawal, while the rest is used to satisfy EFRs as recommended by the FAO.

$$EFRs_{(x,\,t)} = 0.75 \times (TWA_{(x,t)}) \tag{5}$$

where $EFRs_{(x,t)}$ is the environmental flow requirements for district 'x' at period 't'. BW scarcity for district 'x' at period 't' is calculated as the ratio of blue water footprint to BW availability using the following equation:

$$BW_{scarcity} = \frac{Blue\ water\ footprint_{(x,t)}}{Blue\ water\ availability_{(x,t)}} \tag{6}$$

where $BW_{scarcity}$ is the blue water scarcity, $Blue\ water\ footprint_{(x,t)}$ is the blue water footprint for a given district 'x' at period 't', and $Blue\ water\ availability_{(x,t)}$ is the blue water availability for a given district 'x' at period 't'. The blue water footprint for each district was estimated by multiplying the country-wide average per capita water consumption (industry, agriculture, and municipal) by the population of each district. Country-wide water consumption estimates were obtained from FAO AQUASTAT. Population data were obtained from Cameroons' Central Bureau for Census and Population Studies, third national demographic and health survey. To obtain BWA for each district in m^3/year, we converted BWA from mm/year to m/year by dividing by 1,000 and multiplying the value by the total surface area of each district. Table 1 shows the classification of BW scarcity and the Falkenmark index into different classes as suggested by Hoekstra *et al.* (2011) and Falkenmark *et al.* (1989), respectively.

Table 1 | Classification of BW scarcity and the FLK index into different categories

BW			FLK index	
BW scarcity	**Category**	**Interpretation**	**FLK (m^3/capita/year)**	**Threshold/category**
<100%	Low BW scarcity	BWF does not exceed the BWA. The ERF is satisfied at this level.	>1,700	No stress
100–150%	Moderate BW scarcity	BWF is between 20 and 30% of natural runoff. EFR is not satisfied.	1,000–1,700	Stress
150–200%	Significant BW scarcity	BWF is between 30 and 40% of natural runoff. EFR is not satisfied.	500–1,000	Scarcity
>200%	Severe BW scarcity	BWF exceeds 40% of natural runoff. EFR is not satisfied.	<500	Absolute scarcity

BWF, blue water footprint; EFR, environmental flow requirement; FLK, Falkenmark.

The Falkenmark (FLK) index was used to estimate population-driven water scarcity. The index was calculated as the ratio between BWA and the population. The FLK index for district '*x*' was calculated as follows:

$$FLK_{(x)} = \frac{Blue\ water\ availability_{(x)}}{Population_{(x)}} \tag{7}$$

The author is aware of the uncertainties inherent in the different satellite estimates used in this study, which may affect the results obtained, and wishes to accept this as one of the flaws in this study. Another flaw in this study is that the latest population data from Cameroon date as far back as 2005, which may not reflect the current population in the study area.

3. RESULTS

3.1. Climatology

The long-term mean annual and seasonal precipitation derived from CHIRPS v2 over the period 1982–2020 revealed that precipitation over Anglophone Cameroon follows a south–north decreasing gradient (Figure 2(a)). The maximum precipitation was recorded in the southwest around the coastal areas (Ndian and Fako) where annual precipitation exceeds 3,400 mm/year, while the minimum precipitation ranging between 1,800 and 2,200 mm/year was recorded in the northwest (Bui, Donga-Mantung, Mezam, and Ngokentugia) and parts of Lebialem in the southwest region (Figure 2(a)). Seasonal precipitation, JJAS and MAM, follows a pattern similar to annual precipitation (Figure 2(b) and (c)). Furthermore, the results revealed that long-term mean annual and seasonal precipitation vary in the same order of magnitude (6–25%). However, the variability in seasonal precipitation is stronger than annual precipitation, with MAM showing the strongest variability around the coastal areas (Figure 2(d)–(f)).

Figure 3 shows the long-term maximum, minimum, and average surface temperatures based on TC data. The analysis showed that the annual maximum, minimum, and average temperatures in the study area range within 26°–31°, 12°–23°, and 20°–26.5°, respectively (Figure 3(a)–(c)). The analysis further revealed that the lowest temperature was recorded in Oku district, Bui County, while the highest temperature was recorded in Ako district, Donga-Mantung County, in the northwest region. Despite the highest temperature being recorded in the northwest region, it can also be observed that the long-term annual temperature was also substantially high across parts of the southwest region, particularly around the Fako, Manyu, Meme, and Ndian Counties (Figure 3(a)–(c)).

Figure 4 shows the monthly precipitation and temperature climatology in the study area. Long-term mean monthly precipitation analysis showed a unimodal rainfall regime, with the mean monthly precipitation ranging from 100 mm/month to slightly above 350 mm/month. The analysis reveals that peak rainfall occurs from May to October when monthly rainfall exceeds 200 mm/month, maximum and minimum precipitation occurs in August and December, respectively, and there is no precipitation-free month in Anglophone Cameroon (Figure 4(a)). Long-term mean monthly temperature climatology showed that maximum and minimum monthly temperatures were recorded in March and August, respectively, with the dry season lasting from November to April (Figure 4(b)).

3.2. Trend analysis

Figure 5 shows the results of long-term trend in annual and seasonal precipitation across the study area. The analysis indicated a significant decreasing trend (−8 mm/year) in annual precipitation around Akwaya district, Manyu County, while a significant increasing trend (+10 mm/year) was noticed in the coastal areas around Fako County (Figure 5(a)). Similarly, an increasing trend (+7 mm/year) in seasonal precipitation (JJAS) was noticed around Fako County. In contrast, significant decreasing trends (−5 mm/year) in seasonal precipitation (JJAS) were recorded around the Akwaya, Menchum Valley, and Fungom districts (Figure 5(b)). The analysis further revealed that MAM seasonal precipitation remained relatively stable across all districts, with non-significant positive trends recorded around the Menchum Valley, Fungom, and Furu-Awa districts (Menchum County), while non-significant negative trends were obtained around the Lebialem, Manyu, and Momo Counties (Figure 5(c)).

Unlike trends in annual and seasonal precipitation that varied across the study area, there was a consistent increase (0.015–0.030 °C) in annual (max, min, and mean) temperatures across all districts. However, significant increasing trends in the maximum temperature were recorded mostly in the coastal areas (Fako and Ndian Counties) (Figure 6(a)), significant increasing

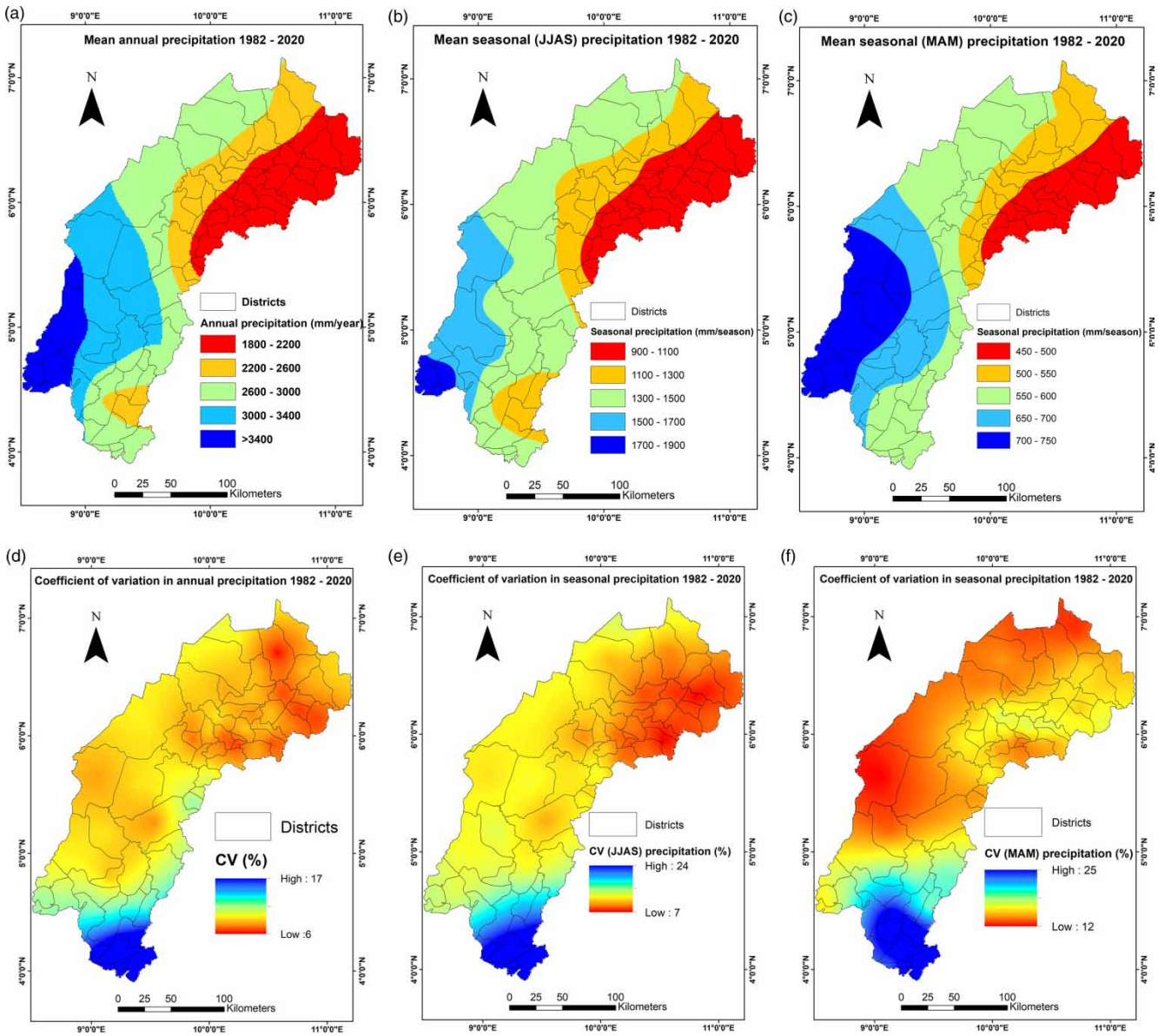

Figure 2 | Spatial distribution of mean precipitation across the study area annual (a) JJAS, (b) MAM, (c) and their respective coefficients of variation (d–f).

trends in the minimum temperature were recorded across the northwest region (Figure 6(b)), and non-significant increasing trends in the average temperature were recorded around the eastern and north-eastern portions of the study area (Figure 6(c)).

3.3. Water security assessments

Figure 7 shows the spatial distribution of annual GW storage (soil moisture), GW flow (AET), and BWA (*P*–AET) across all districts. The analysis revealed that GW storage varied between 750 and 950 mm/year, except in a few districts where GW storage was either below or above this range (Figure 7(a)). The analysis also revealed that GW flow (AET) was substantially higher in the southwest (1,200–1,600 mm/year) than in the northwest (800–1,200 mm/year) (Figure 7(b)). Areas with the lowest BWA are located in the north-eastern part of the study area, while BWA was substantially high across the coastal area (Figure 7(c)).

Water scarcity assessment was carried out using three different metrics, namely green and blue water footprints and the FLK index. The spatial distribution of the different water scarcity metrics is shown in Figure 8. The analysis revealed that

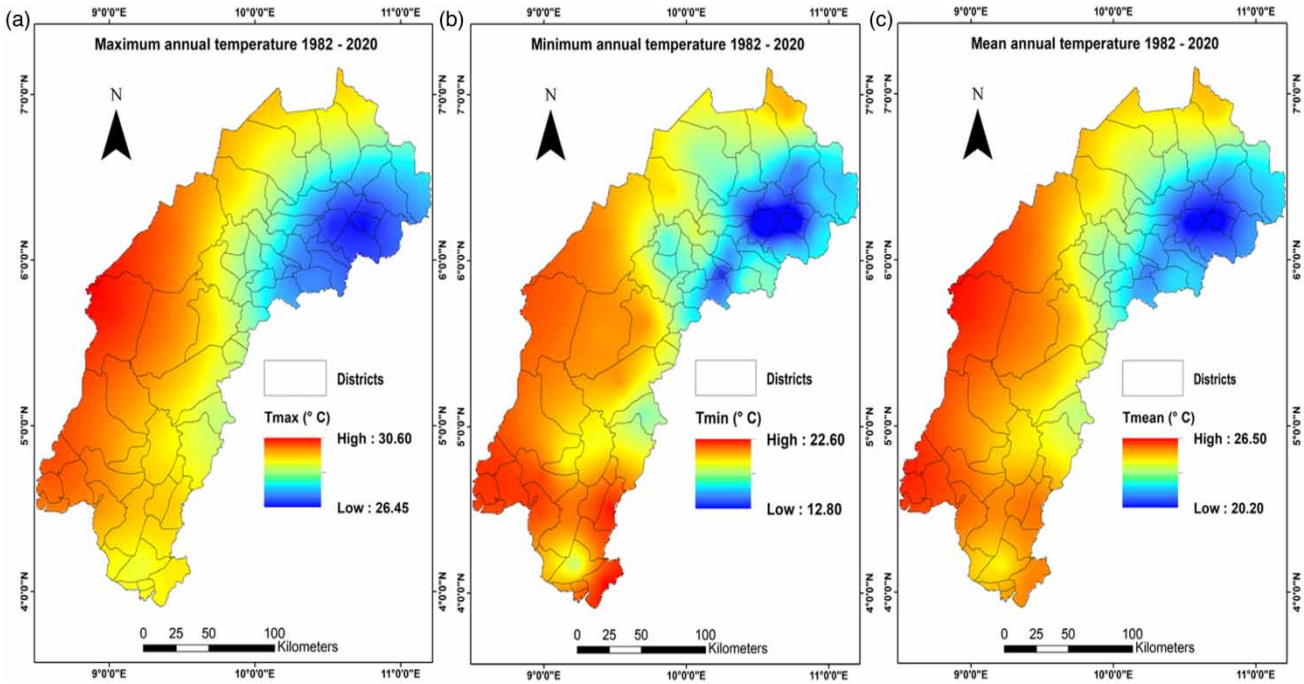

Figure 3 | Spatial distribution of annual temperature across the study area (a) maximum temperature, (b) minimum temperature, and (c) mean temperature.

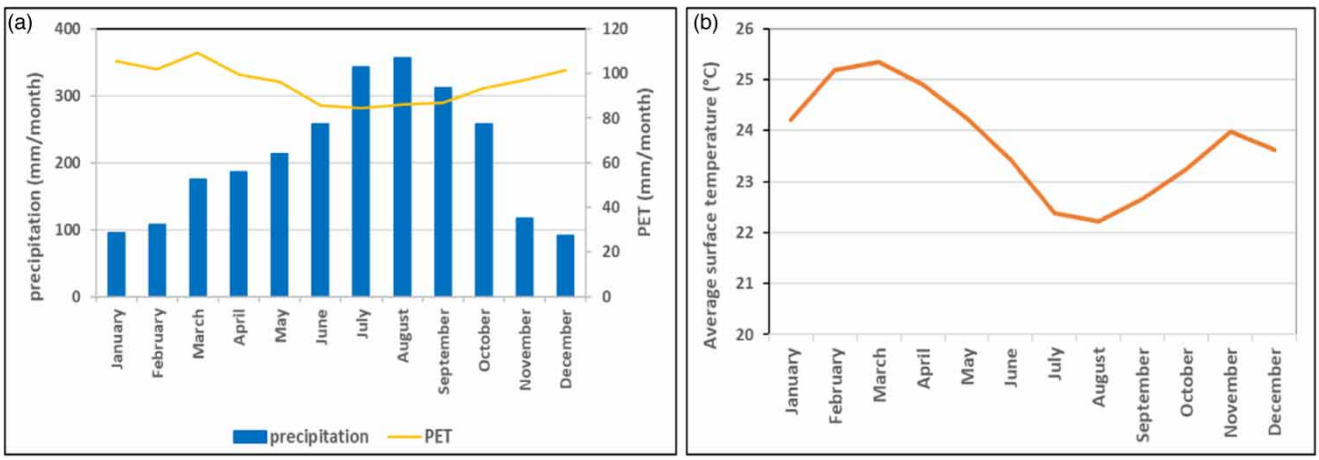

Figure 4 | Long-term mean monthly (a) precipitation and potential evapotranspiration and (b) temperature climatology in the study area.

GW scarcity in the study area varied between 100 and 160%, exceeding 300% in only two districts (Figure 8(a)). Districts where GW scarcity exceeded 160% were mostly located in the creeks and wetland areas such as the Bakassi peninsular (southwest region) and Ndop plain (northwest region). BW scarcity was also substantially low (0–5%) across the study area, exceeding 25% in only one district (Figure 8(b)). BW scarcity across all districts can, therefore, be categorised as low according to Table 1.

The results of the FLK index showed that population-driven water scarcity is substantially low across most districts. Nevertheless, this does not appear to be the case in some districts in Fako, Lebialem, Mezam, Nogketungia, and Bui Counties where annual per capita water availability was estimated to be less than 1,700 m^3/capita/year (Figure 8(c)). In these districts, population-driven water scarcity can be described as ranging from stress to absolute scarcity in some districts. However, per capita water availability was substantially high in other counties with low-population density, such as Ndian, Manyu, and Menchum.

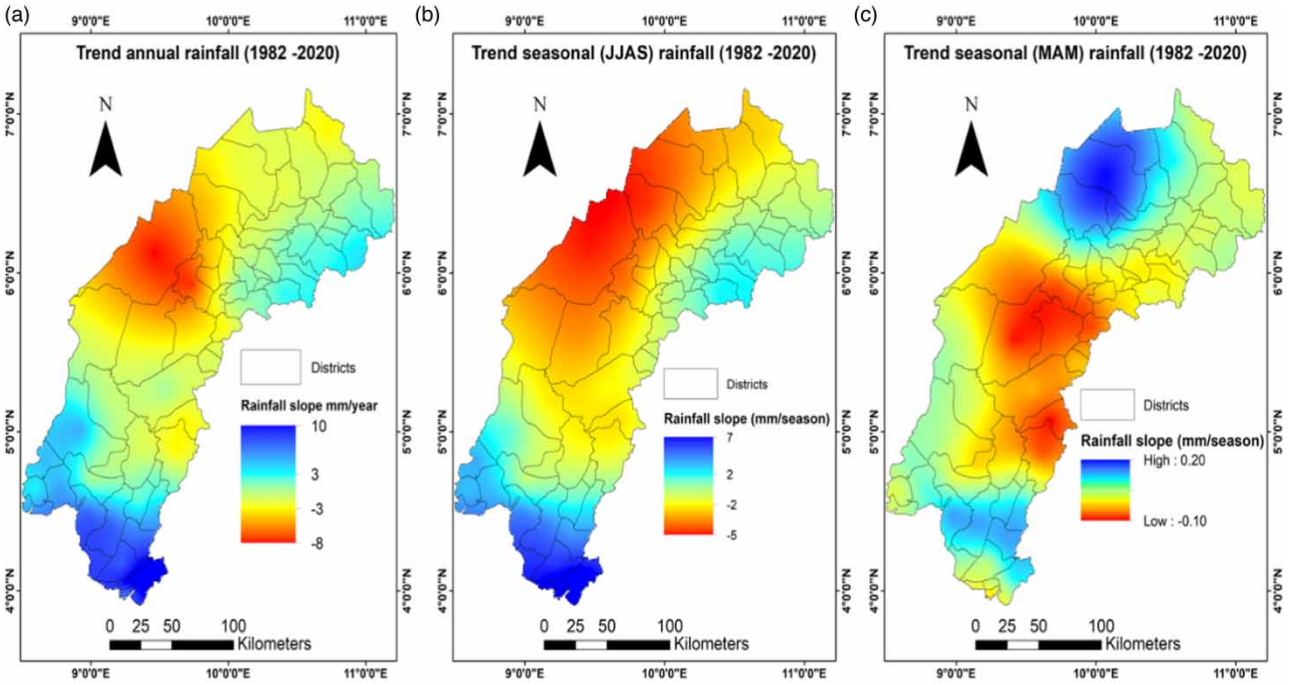

Figure 5 | Precipitation trends across the study area (a) annual, (b) JJAS, and (c) MAM.

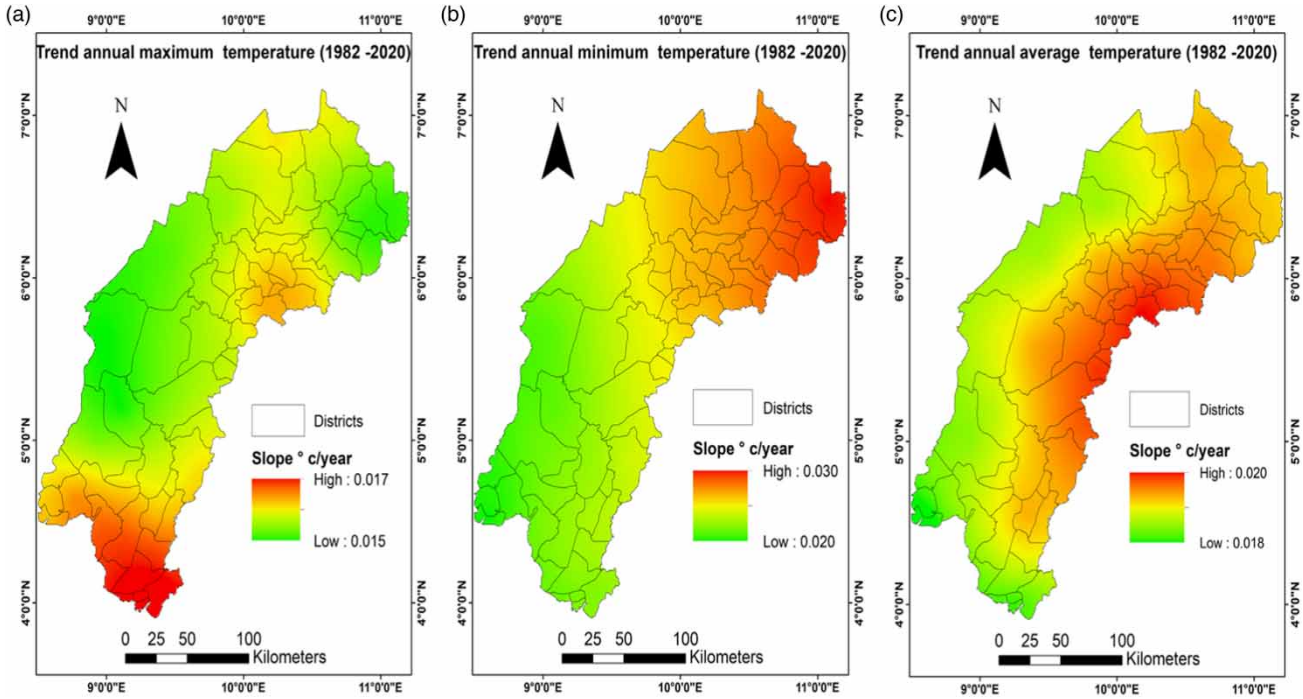

Figure 6 | Long-term trends in annual (a) maximum temperature, (b) minimum temperature, and (c) average temperature.

From Table 1 and Figure 8(b), it is safe to suggest that BW scarcity is yet to become a major challenge in the study area because the blue water footprint does not exceed BWA, given that BW scarcity is far below 100%. This implies that in theory, most districts can still meet their water demands and EFRs. The classification of the FLK index in Table 1 also suggests

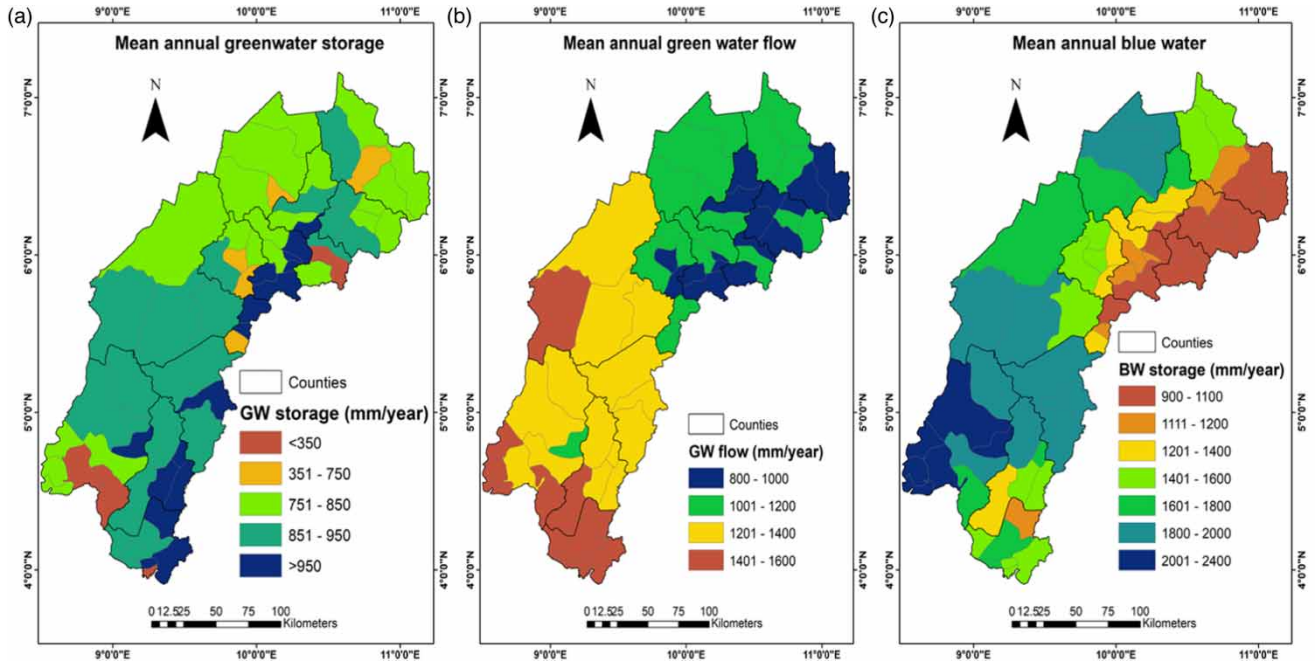

Figure 7 | Spatial distribution of mean annual (a) GW storage (soil moisture), (b) GW flow (AET), and (c) BW resources (*P–AET*).

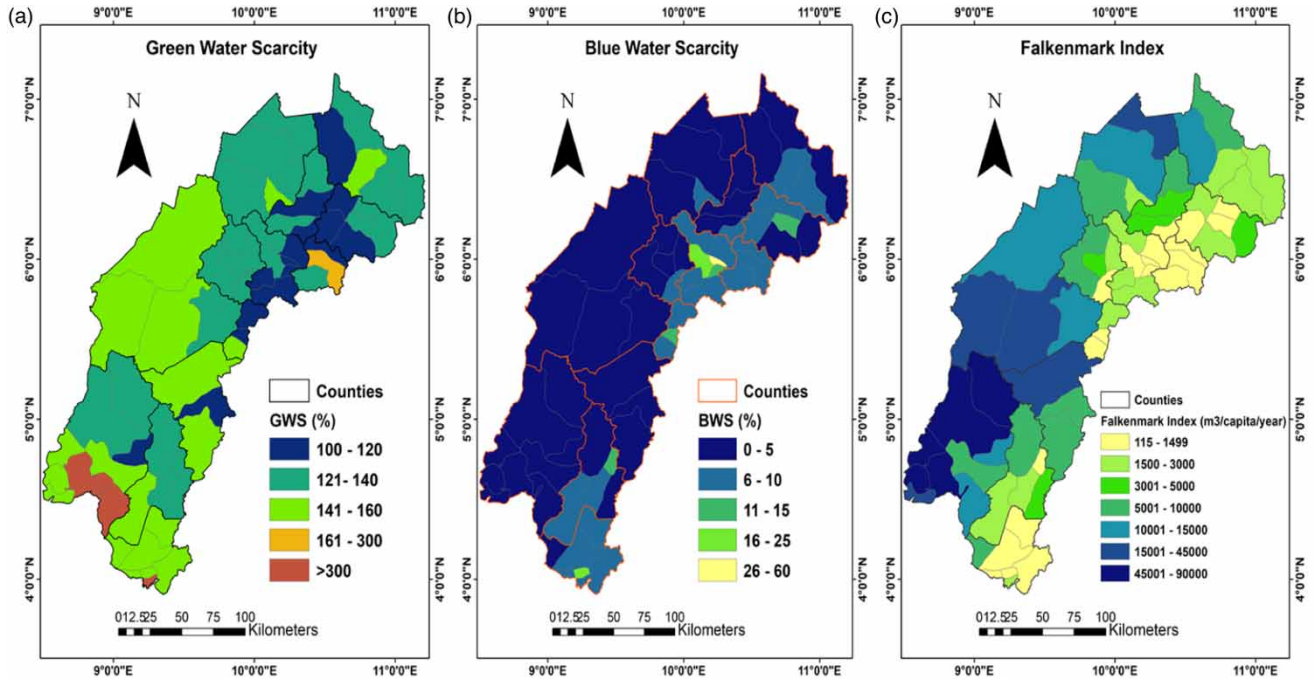

Figure 8 | Spatial distribution of (a) mean annual GW scarcity, (b) BW scarcity, and (c) the FLK index.

that most districts fall under the 'no stress' category. This suggests that the available water resources can satisfy the demands of the population in most districts, except in areas with a high population density.

4. DISCUSSION

The results of the trend analysis from this study are similar to those obtained from regional-scale studies covering Cameroon. However, this study employed high spatial resolution data, which offers the opportunity to focus on local changes in more

detail than regional-scale analysis. Local-scale analysis reported herein provides a clear visualisation of spatial trends in hydroclimatic variables at a high spatial resolution, which can help to identify water scarcity hotspots.

4.1. Climatology

Precipitation analysis indicated that the southwest is wetter than the northwest, whereas the temperature analysis revealed that Oku (Bui County) and Ako (Donga-Mantung County) are, respectively, the coldest and hottest districts in Anglophone Cameroon. The south–north precipitation gradient observed in the study area is consistent with the results from other studies in Cameroon (Nkiaka *et al.* 2017). Precipitation estimates from CHIRPS v2 appear to be consistent with gauge estimates in parts of the study area (Awazi *et al.* 2019). Annual precipitation elsewhere in the region is estimated to reach 10,000 mm/year in Debuncha, making it the wettest place in Cameroon and one of the wettest places in the world (Feka *et al.* 2011).

High variability in annual and seasonal precipitation around the coastal areas can be attributed to several factors, including orographic effects caused by the massive Fako Mountain, the proximity of the Atlantic Ocean, which creates a land–sea interface, and the dense vegetation around the coast, which contributes to the formation of a zone of moisture convergence around this area (Vondou *et al.* 2018; Worou *et al.* 2020). Modest variability (0–25%) in annual precipitation indicates low variability in annual GW storage (soil moisture) and BWA. However, this may not be the case at the monthly time scale, given the strong variability in monthly precipitation in the study area. Precipitation climatology also showed that there is no precipitation-free month in the study area, which is consistent with the analysis from the other regions of Cameroon (Evariste *et al.* 2018). However, unlike the rest of the southern portion of Cameroon with a bimodal rainfall, our analysis revealed a unimodal rainfall regime over Anglophone Cameroon. Mean annual temperature climatology is consistent with the analysis from other studies in Anglophone Cameroon (Awazi *et al.* 2019), thereby lending some credibility to TC temperature estimates.

4.2. Precipitation and temperature trend analysis

Precipitation trend analysis shows both statistically significant increasing and decreasing trends in annual and seasonal precipitation across different parts of the study area. Significant positive trends in precipitation were recorded in the coastal areas, which are consistent with the results from other studies in the Gulf of Guinea (Nkrumah *et al.* 2019). Increasing trends in precipitation around the Gulf of Guinea and further inland have been attributed to the intensification of mesoscale convective systems in the region (Nkrumah *et al.* 2019). Increasing precipitation in the coastal areas has significant implications for flooding, which is reported to be increasing in this part of the study area (Ajonina *et al.* 2021). Conversely, significant decreasing trends in annual precipitation in Akwaya seem to follow a similar pattern observed in Eyumodjock, which is a neighbouring district (Ngalim & Besong 2020). Decreasing precipitation in parts of the northwest also appears to follow a similar pattern observed across the Sudano-Savannah zone of Cameroon (Nkiaka *et al.* 2017; Njouenwet *et al.* 2021).

Decreasing precipitation in parts of the northwest has been attributed to a decrease in the number of rainy days and the length of the rainy season, leading to a cumulative decrease in annual precipitation with a significant impact on water availability (Sedrique & Nfor 2020; Tume 2021). However, while annual precipitation has been declining, other studies have reported an increase in the frequency of extreme precipitation in the northwest, resulting in an increase in flooding in urban areas and low-lying areas like Ndop (Saha & Tchindjang 2017; Kometa 2019).

Temperature trends follow a similar pattern reported in other parts of Anglophone Cameroon, e.g., Manyu (Ngalim & Besong 2020) and the Bamenda (Nyong *et al.* 2019). Trend magnitudes obtained in this study are consistent with the results from other regional-scale assessments using CRU4.0 (Iyakaremye *et al.* 2021) and across West Africa using TC temperature data (Muthoni 2020). Increasing temperatures in the study area will likely increase the evaporative demand for water as demonstrated by Gosling & Arnell (2016), thereby enhancing evapotranspiration with a likely knock-on effect on soil moisture and BWA.

4.3. Water security assessment

The results from the study indicated that GW flow was higher in the southwest than in the northwest region. In fact, the higher GW flow in the southwest can be attributed to a higher percentage of forest and extensive swaths of rubber, banana, palm oil, cocoa, and plantain plantations. As such, even in periods of low precipitation, the dense vegetation is

still able to extract water from the deeper layers of the soil to sustain evapotranspiration. This is consistent with the results from other studies in Africa reporting that areas covered by a high percentage of forest are able to enhance evapotranspiration even in the dry season (Mwangi *et al.* 2016). Enhanced evapotranspiration can also be attributed to increasing temperatures, thereby increasing the atmospheric demand for water (Gosling & Arnell 2016).

Demand-driven BW scarcity from irrigation agriculture and industries is substantially low because of low BW withdrawal, given that most of the agriculture in the study area is rainfed. In addition, there are no industries that withdraw substantial amounts of BW. Therefore, most of the BW withdrawal is for domestic purposes. BW scarcity in the study area can, therefore, be categorised as low across most districts. Conversely, population-driven water scarcity in some districts is substantially high. This can be linked to high population density in towns such as Limbe, Buea, Tiko, Mutengene, and Muyuka (Fako), Kumba (Meme), Bamenda (Mezam), and Kumbo (Bui). This high population density exerts significant pressure on BWA, thereby reducing the per capita water availability in those districts. Previous studies have also highlighted population-driven water scarcity to be a major cause for concern in other countries (Brown *et al.* 2019; Veettil & Mishra 2020). From our analyses, the most water-stressed counties in Anglophone Cameroon are Fako, Meme, and Lebialem in the southwest and Bui, Mezam, and Ngokentungia in the northwest.

Although the results from the study show that BW scarcity does not appear to be a major challenge in the study area, except in the densely populated districts, this does not imply that the population has access to this water. In fact, access to water services remains very low in Anglophone Cameroon, like in several parts of sub-Saharan Africa (Nkiaka *et al.* 2021b). Overall, the results from this study suggest that BW scarcity does not appear to be a major cause for concern yet in the study area, which implies that EFRs can readily be satisfied. Therefore, it is very likely that SDG 6.4 (water stress) and 6.6 (ecosystems) may be achieved in the study area.

5. CONCLUSIONS

The overarching goal of this study was to show how to assess water security in ungauged regions using the water balance and water footprint concepts and satellite observations. This goal is in line with the 'Panta Rhei' initiative to use advanced monitoring and data analysis techniques to address water security challenges at different scales (Montanari *et al.* 2013). Considering the availability of a wide range of free satellite data, our results suggest that the proposed methodology can be used to assess water security in other ungauged regions.

While precipitation analysis returned trends with varying strengths and magnitudes for different districts, temperature analysis revealed significant increasing trends across all districts. This suggests that global warming may be a key driver of water scarcity in the study area, which could increase the future demand for water (Gosling & Arnell 2016). Our results also indicated that population-driven water scarcity is more apparent in the urban areas with a high population density than in districts with a low-population density. These findings are in line with recent calls to identify the factors driving water scarcity at the local scale in Africa (Nkiaka *et al.* 2021a).

Although several hydrological modelling studies have been conducted in Africa to assess water availability, only a few studies have focused on assessing blue and green water scarcities and the drivers of water scarcity at the district level. This is probably the first study in Africa to conduct a multiscale water security assessment covering all administrative units from the district, county to a regional scale within the same country. Another novelty is the use of an integrated approach that adopts different indicators to assess water security based on the needs of different stakeholders. Unlike previous water security assessments that have focused on global and regional scales, thereby concealing spatial heterogeneity that exists within countries, the present study has adopted a more localised approach, thereby unmasking districts that are vulnerable to water scarcity.

The results from this study will benefit national- to district-level stakeholders involved in water, agriculture, and disaster management by helping them to identify districts where urgent attention may be needed to devise more water and disaster management strategies. Districts with high GW availability or storage may be favourable for agricultural expansion to reduce food security. Future research will seek to incorporate climate and land-use changes in water security assessments, thus allowing for early identification of specific districts where water conflicts may arise due to water scarcity. There is also a need to understand the impact of monoculture crops like banana, plantain, rubber, and cocoa on evapotranspiration and how this may affect water security in the long term.

ACKNOWLEDGEMENTS

E.N. received funds from the Leverhulme Trust Early Career Fellowship – Award Number ECF – 097 – 2020. All the datasets used in this study are freely available as indicated in the manuscript.

AUTHOR'S CONTRIBUTIONS

E.N. conceptualised the study, performed data curation, prepared the methodology, did the formal analysis, and wrote the original draft.

CONFLICT OF INTEREST STATEMENT

The author declares no conflict of interest in this study.

DATA AVAILABILITY STATEMENT

All relevant data are available from an online repository or repositories https://climateserv.servirglobal.net TerraClimate www.climatologylab.org/terraclimate.html GLEAM www.gleam.eu.

REFERENCES

Abatzoglou, J. T., Dobrowski, S. Z., Parks, S. A. & Hegewisch, K. C. 2018 TerraClimate, a high-resolution global dataset of monthly climate and climatic water balance from 1958–2015. *Scientific Data* **5**, 1–12. doi:10.1038/sdata.2017.191.

Ajonina, U. P., Joseph, T. N. & Meh, C. L. 2021 Assessing flood vulnerability index for policy implications towards flood risk management along the Atlantic Coast of Limbe, Cameroon. *American Journal of Water Science and Engineering* **7**, 24–38. doi:10.11648/j.ajwse.20210702.11.

Alemu, M. M. & Bawoke, G. T. 2020 Analysis of spatial variability and temporal trends of rainfall in Amhara region, Ethiopia. *Journal of Water and Climate Change* **11**, 1505–1520. https://doi.org/10.2166/wcc.2019.084.

Awazi, N. P., Tchamba, M. N. & Avana, T. M.-L. 2019 Climate change resiliency choices of small-scale farmers in Cameroon: determinants and policy implications. *Journal of Environmental Management* **250**, 109560. https://doi.org/10.1016/j.jenvman.2019.109560.

Baggio, G., Qadir, M. & Smakhtin, V. 2021 Freshwater availability status across countries for human and ecosystem needs. *Science of The Total Environment* 148230. https://doi.org/10.1016/j.scitotenv.2021.148230.

Boulay, A. M., Bare, J., Benini, L., Berger, M., Lathuillière, M. J., Manzardo, A., Margni, M., Motoshita, M., Núñez, M., Pastor, A. V. & Ridoutt, B. 2018 The WULCA consensus characterization model for water scarcity footprints: assessing impacts of water consumption based on available water remaining (AWARE). *The International Journal of Life Cycle Assessment* **23**, 368–378.

Brown, T. C., Mahat, V. & Ramirez, J. A. 2019 Adaptation to future water shortages in the United States caused by population growth and climate change. *Earth's Future* **7**, 219–234. https://doi.org/10.1029/2018EF001091.

D'Ambrosio, E., Ricci, G. F., Gentile, F. & De Girolamo, A. M. 2020 Using water footprint concepts for water security assessment of a basin under anthropogenic pressures. *Science of the Total Environment* **748**, 141356. https://doi.org/10.1016/j.scitotenv.2020.141356.

Dembélé, M., Ceperley, N., Zwart, S. J., Salvadore, E., Mariethoz, G. & Schaefli, B. 2020 Potential of satellite and reanalysis evaporation datasets for hydrological modelling under various model calibration strategies. *Advances in Water Resources* **143**, 103667. https://doi.org/10.1016/j.advwatres.2020.103667.

Dinku, T., Funk, C., Peterson, P., Maidment, R., Tadesse, T., Gadain, H. & Ceccato, P. 2018 Validation of the CHIRPS satellite rainfall estimates over eastern Africa. *Quarterly Journal of the Royal Meteorological Society* **144**, 292–312. https://doi.org/10.1002/qj.3244.

Elagib, N. A., Al Zayed, I. S., Saad, S. A. G., Mahmood, M. I., Basheer, M. & Fink, A. H. 2021 Debilitating floods in the Sahel are becoming frequent. *Journal of Hydrology* **599**, 126362. https://doi.org/10.1016/j.jhydrol.2021.126362.

Evariste, F. F., Jean, S. D., Victor, K. & Claudia, M. 2018 Assessing climate change vulnerability and local adaptation strategies in adjacent communities of the Kribi-Campo coastal ecosystems, South Cameroon. *Urban Climate* **24**, 1037–1051. https://doi.org/10.1016/j.uclim.2017.12.007.

Falkenmark, M., Lundqvist, J. & Widstrand, C. 1989 Macro-scale water scarcity requires micro-scale approaches: aspects of vulnerability in semi-arid development. *Natural Resources Forum* **13**, 258–267. https://doi.org/10.1111/j.1477-8947.1989.tb00348.x.

Feka, N. Z., Manzano, M. G. & Dahdouh-Guebas, F. 2011 The effects of different gender harvesting practices on mangrove ecology and conservation in Cameroon. *International Journal of Biodiversity Science, Ecosystem Services & Management* **7**, 108–121. https://doi.org/10.1080/21513732.2011.606429.

Flörke, M., Schneider, C. & McDonald, R. I. 2018 Water competition between cities and agriculture driven by climate change and urban growth. *Nature Sustainability* **1**, 51–58. https://doi.org/10.1038/s41893-017-0006-8.

Funk, C., Peterson, P., Landsfeld, M., Pedreros, D., Verdin, J., Shukla, S., Husak, G., Rowland, J., Harrison, L., Hoell, A. & Michaelsen, J. 2015 The climate hazards infrared precipitation with stations – a new environmental record for monitoring extremes. *Scientific Data* **2**, 1–21. https://doi.org/10.1038/sdata.2015.66.

Gosling, S. N. & Arnell, N. W. 2016 A global assessment of the impact of climate change on water scarcity. *Climatic Change* **134**, 371–385. https://doi.org/10.1007/s10584-013-0853-x.

Hailu, R., Tolossa, D. & Alemu, G. 2019 Water security: stakeholders' arena in the Awash River Basin of Ethiopia. *Sustainable Water Resources Management* **5**, 513–531. https://doi.org/10.1007/s40899-017-0208-2.

Halbwachs, M., Sabroux, J. C. & Kayser, G. 2020 Final step of the 32-year Lake Nyos degassing adventure: Natural CO_2 recharge is to be balanced by discharge through the degassing pipes. *Journal of African Earth Sciences* **167**, 103575. https://doi.org/10.1016/j.jafrearsci.2019.103575.

Hoekstra, A. Y. 2017 Water footprint assessment: evolvement of a new research field. *Water Resources Management* **31**, 3061–3081. https://doi.org/10.1007/s11269-017-1618-5.

Hoekstra, A. Y., Chapagain, A. K., Mekonnen, M. M. & Aldaya, M. M. 2011 *The Water Footprint Assessment Manual: Setting the Global Standard*. Routledge, London.

ISO, I.O.f.S. 2014 *Environmental Management: Water Footprint–Principles, Requirements and Guidelines*. International Organization for Standardization, Geneva.

Iyakaremye, V., Zeng, G., Siebert, A. & Yang, X. 2021 Contribution of external forcings to the observed trend in surface temperature over Africa during 1901–2014 and its future projection from CMIP6 simulations. *Atmospheric Research* **254**, 105512. https://doi.org/10.1016/j.atmosres.2021.105512.

Jaramillo, F., Cory, N., Arheimer, B., Laudon, H., Van Der Velde, Y., Hasper, T. B., Teutschbein, C. & Uddling, J. 2018 Dominant effect of increasing forest biomass on evapotranspiration: interpretations of movement in Budyko space. *Hydrology and Earth System Sciences* **22**, 567–580.

Khosa, F. V., Mateyisi, M. J., Merwe, M. R. v. d., Feig, G. T., Engelbrecht, F. A. & Savage, M. J. 2020 Evaluation of soil moisture from CCAM-CABLE simulation, satellite-based models estimates and satellite observations: a case study of Skukuza and Malopeni flux towers. *Hydrology and Earth System Sciences* **24**, 1587–1609. https://doi.org/10.5194/hess-24-1587-2020.

Kometa, C. G. 2019 Climate change evolution and indigenous methods of flood control in the Upper Nun Valley of Cameroon. *American Journal of Traffic and Transportation Engineering* **4**, 56–66. doi:10.11648/j.ajtte.20190402.13.

Larbi, I., Hountondji, F. C., Dotse, S. Q., Mama, D., Nyamekye, C., Adeyeri, O. E., Djan'na Koubodana, H., Odoom, P. R. E. & Asare, Y. M. 2020 Local climate change projections and impact on the surface hydrology in the Vea catchment, West Africa. *Hydrology Research*. https://doi.org/10.2166/nh.2021.096.

Majozi, N. P., Mannaerts, C. M., Ramoelo, A., Mathieu, R., Mudau, A. E. & Verhoef, W. 2017 An intercomparison of satellite-based daily evapotranspiration estimates under different eco-climatic regions in South Africa. *Remote Sensing* **9**, 307. https://doi.org/10.3390/rs9040307.

Martens, B., Miralles, D. G., Lievens, H., Van Der Schalie, R., De Jeu, R. A., Fernández-Prieto, D., Beck, H. E., Dorigo, W. A. & Verhoest, N. E. 2017 GLEAM v3: satellite-based land evaporation and root-zone soil moisture. *Geoscientific Model Development* **10**, 1903–1925. https://doi.org/10.5194/gmd-10-1903-2017.

Mekonnen, M. M. & Hoekstra, A. Y. 2016 Four billion people facing severe water scarcity. *Science Advances* **2**, e1500323. doi:10.1126/sciadv.1500323.

Montanari, A., Young, G., Savenije, H. H. G., Hughes, D., Wagener, T., Ren, L. L., Koutsoyiannis, D., Cudennec, C., Toth, E., Grimaldi, S. & Blöschl, G. 2013 'Panta Rhei – everything flows': change in hydrology and society – the IAHS scientific decade 2013–2022. *Hydrological Sciences Journal* **58**, 1256–1275. https://doi.org/10.1080/02626667.2013.809088.

Muthoni, F. 2020 Spatial-temporal trends of rainfall, maximum and minimum temperatures over West Africa. *IEEE Journal of Selected Topics in Applied Earth Observations and Remote Sensing* **13**, 2960–2973. doi:10.1109/JSTARS.2020.2997075.

Muthoni, F. K., Odongo, V. O., Ochieng, J., Mugalavai, E. M., Mourice, S. K., Hoesche-Zeledon, I., Mwila, M. & Bekunda, M. 2019 Long-term spatial-temporal trends and variability of rainfall over Eastern and Southern Africa. *Theoretical and Applied Climatology* **137**, 1869–1882. https://doi.org/10.1007/s00704-018-2712-1.

Mwangi, H. M., Julich, S., Patil, S. D., McDonald, M. A. & Feger, K.-H. 2016 Modelling the impact of agroforestry on hydrology of Mara River Basin in East Africa. *Hydrological Processes* **30**, 3139–3155.

Ngalim, R. N. M. & Besong, T. P. 2020 Climate variability and food crop production in rural Cameroon: the case of Ejagham Community-Manyu Division. *International Journal of Environment and Climate Change* 60–77. doi:10.9734/IJECC/2020/v10i330188.

Njouenwet, I., Vondou, D. A., Dassou, E. F., Ayugi, B. O. & Nouayou, R. 2021 Assessment of agricultural drought during crop-growing season in the Sudano–Sahelian region of Cameroon. *Natural Hazards* **106**, 561–577. https://doi.org/10.1007/s11069-020-04475-x.

Nkiaka, E., Nawaz, N. & Lovett, J. 2017 Analysis of rainfall variability in the Logone catchment, Lake Chad basin. *International Journal of Climatology* **37**, 3553–3564. https://doi.org/10.1002/joc.4936.

Nkiaka, E., Bryant, R. G., Okumah, M. & Gomo, F. F. 2021a Water security in sub-Saharan Africa: understanding the status of sustainable development goal 6. *WIREs Water* **8**, e1552. https://doi.org/10.1002/wat2.1552.

Nkiaka, E., Okpara, U. T. & Okumah, M. 2021b Food-energy-water security in sub-Saharan Africa: quantitative and spatial assessments using an indicator-based approach. *Environmental Development* 100655. https://doi.org/10.1016/j.envdev.2021.100655.

Nkrumah, F., Vischel, T., Panthou, G., Klutse, N. A. B., Adukpo, D. C. & Diedhiou, A. 2019 Recent trends in the daily rainfall regime in southern West Africa. *Atmosphere* **10**, 741. https://doi.org/10.3390/atmos10120741.

Nyong, A. P., Ngankam, T. M. & Felicite, T. L. 2019 Enhancement of resilience to climate variability and change through agroforestry practices in smallholder farming systems in Cameroon. *Agroforestry Systems* 1–19. https://doi.org/10.1007/s10457-019-00435-y.

Odusanya, A. E., Mehdi, B., Schürz, C., Oke, A. O., Awokola, O. S., Awomeso, J. A., Adejuwon, J. O. & Schulz, K. 2019 Multi-site calibration and validation of SWAT with satellite-based evapotranspiration in a data-sparse catchment in southwestern Nigeria. *Hydrology and Earth System Sciences* **23**, 1113–1144. https://doi.org/10.5194/hess-23-1113-2019.

Peel, M. C., Finlayson, B. L. & McMahon, T. A. 2007 Updated world map of the Köppen-Geiger climate classification. *Hydrology and Earth System Sciences* **11**, 1633–1644.

Quinteiro, P., Rafael, S., Vicente, B., Marta-Almeida, M., Rocha, A., Arroja, L. & Dias, A. C. 2019 Mapping green water scarcity under climate change: a case study of Portugal. *Science of The Total Environment* **696**, 134024.

Rodrigues, D. B., Gupta, H. V. & Mendiondo, E. M. 2014 A blue/green water-based accounting framework for assessment of water security. *Water Resources Research* **50**, 7187–7205. https://doi.org/10.1002/2013WR014274.

Rungee, J., Ma, Q., Goulen, M. & Bales, R. 2021 Evapotranspiration and runoff patterns across California's Sierra Nevada. *Frontiers in Water* **3**, 150.

Saha, F. & Tchindjang, M. 2017 Rainfall variability and floods occurrence in the city of Bamenda (northwest of Cameroon). *Present Environment and Sustainable Development* 65–82. https://doi.org/10.1515/pesd-2017-0006.

Satgé, F., Defrance, D., Sultan, B., Bonnet, M. P., Seyler, F., Rouche, N., Pierron, F. & Paturel, J. E. 2020 Evaluation of 23 gridded precipitation datasets across West Africa. *Journal of Hydrology* **581**, 124412. https://doi.org/10.1016/j.jhydrol.2019.124412.

Sedrique, Z. T. & Nfor, J. T. 2020 Rainfall variability and quantity of water supply in Bamenda I, Northwest Region of Cameroon. In: *African Handbook of Climate Change Adaptation*. pp. 1–21. https://doi.org/10.1007/978-3-030-42091-8_139-1.

Sheffield, J., Wood, E. F., Pan, M., Beck, H., Coccia, G., Serrat-Capdevila, A. & Verbist, K. 2018 Satellite remote sensing for water resources management: potential for supporting sustainable development in data-poor regions. *Water Resources Research* **54**, 9724–9758.

Simons, G., Bastiaanssen, W., Ngo, L. A., Hain, C. R., Anderson, M. & Senay, G. 2016 Integrating global satellite-derived data products as a pre-analysis for hydrological modelling studies: a case study for the Red River Basin. *Remote Sensing* **8**, 279.

Spellman, P., Pritt, A. & Salazar, N. 2021 Tracking changing water budgets across the Bahamian archipelago. *Journal of Hydrology* **598**, 126178. https://doi.org/10.1016/j.jhydrol.2021.126178.

Tramblay, Y., Villarini, G., El Khalki, E. M., Gründemann, G. & Hughes, D. 2021 Evaluation of the drivers responsible for flooding in Africa. *Water Resources Research* **57**, e2021WR029595.

Tume, S. J. P. 2021 Rainfall seasonality and standardized precipitation valuation of water resources susceptibility to climate variability on the Bui Plateau, Northwest Region, Cameroon. *Advances in Hydrology & Meteorology* **1** (1), 1–16.

Veettil, A. V. & Mishra, A. 2020 Water security assessment for the contiguous United States using water footprint concepts. *Geophysical Research Letters* **47**, e2020GL087061. https://doi.org/10.1029/2020GL087061.

Vondou, D. A., Yepdo, Z. D. & Tchotchou, L. D. 2018 Diurnal cycle of convective cloud occurrences over Cameroon during June–August. *Journal of the Indian Society of Remote Sensing* **46**, 829–845. https://doi.org/10.1007/s12524-017-0747-x.

Weerasinghe, I., Bastiaanssen, W., Mul, M., Jia, L. & Griensven, A. v. 2020 Can we trust remote sensing evapotranspiration products over Africa? *Hydrology and Earth System Sciences* **24**, 1565–1586. https://doi.org/10.5194/hess-24-1565-2020.

Worou, K., Goosse, H., Fichefet, T., Guichard, F. & Diakhate, M. 2020 Interannual variability of rainfall in the Guinean Coast region and its links with sea surface temperature changes over the twentieth century for the different seasons. *Climate Dynamics* **55**, 449–470. https://doi.org/10.1007/s00382-020-05276-5.

Xie, J., Xu, Y.-P., Guo, Y. & Wang, Y. 2021 Detecting the dominant contributions of runoff variance across the source region of the Yellow River using a new decomposition framework. *Hydrology Research*. https://doi.org/10.2166/nh.2021.179.

Yang, X., Yong, B., Yin, Y. & Zhang, Y. 2018 Spatio-temporal changes in evapotranspiration over China using GLEAM_V3.0a products (1980–2014). *Hydrology Research* **49**, 1330–1348.

First received 23 November 2021; accepted in revised form 4 February 2022. Available online 15 February 2022